

1       **An assessment of extra-tropical cyclone precipitation**  
2       **extremes over the Southern Hemisphere using ERA5**

3       **Cameron McErlich<sup>1</sup>, Adrian McDonald<sup>1,2</sup>, James Renwick<sup>3</sup>, and Alex**  
4       **Schuddeboom<sup>1</sup>**

5       <sup>1</sup>School of Physical and Chemical Sciences, University of Canterbury, Christchurch, New Zealand

6       <sup>2</sup>Gateway Antarctica, University of Canterbury, Christchurch, New Zealand

7       <sup>3</sup>Victoria University of Wellington, School of Geography, Environment and Earth Science, Wellington,  
8       New Zealand

9       **Key Points:**

- 10       • We detail a new methodology to assess precipitation extremes within cyclone com-  
11       posites using a spatially dependent precipitation threshold
- 12       • Extreme precipitation occurs preferentially and makes up a larger fraction of to-  
13       tal accumulation before cyclones reach maximum depth
- 14       • As extremes increase in intensity precipitation is constrained closer to the cyclone  
15       centre and weakens more rapidly as the cyclone evolves

---

Corresponding author: Cameron McErlich, [cameron.mcerlich@pg.canterbury.ac.nz](mailto:cameron.mcerlich@pg.canterbury.ac.nz)

## Abstract

ERA5 reanalysis is used to examine extreme precipitation using a spatially dependent precipitation threshold applied within a cyclone compositing framework. This is used to account for regional variation in precipitation generating processes within Southern Hemisphere mid-latitude cyclones across the cyclone lifecycle. The spatial extent of extreme precipitation is limited to a smaller region around the cyclone centre compared to non-extreme precipitation, though extreme precipitation displays a good spatial correlation with non-extreme precipitation. Extreme precipitation occurs more often during the deepening phase of the cyclone before it reaches a maximum depth. Precipitation occurrence at the 90th and 98th percentiles reduces to 46% and 30% of the deepening value across the cyclone lifecycle, averaged over the composite. Precipitation fraction at the 90th and 98th percentile reduces to 80% and 60% of the deepening value. Our methodology provides a quantitative assessment of precipitation extremes both spatially and temporally, within a cyclone compositing framework.

## Plain Language Summary

Extra-tropical cyclones play a major role in the circulation within the atmosphere, acting to transfer heat towards the poles. Here we assess the representation of extreme precipitation within extra-tropical cyclones. By applying a threshold for precipitation that changes with geographic location, we are able to determine how extreme precipitation varies within a cyclone-centred coordinate system. When breaking cyclones into lifecycle stages representing deepening, peak intensity and decay, we find that extreme precipitation occurs most often as the cyclone is developing. The area of the cyclone relevant for extremes reduces towards the cyclone centre as the threshold for determining extreme precipitation increases. Extreme precipitation weakens at a higher rate as cyclones become more intense, highlighting the importance of extremes in the growth phase of the cyclone.

## 1 Introduction

Climate change is experienced by society through a variety of ways, including extreme weather events. Unlike long term climate trends which seem distant and occur more gradually, extremes are direct and occur in everyday life. Howe et al. (2014) suggests that people tend to accurately recall and report experiences with extreme weather, with increasing likelihood based on proximity and magnitude of an event. The impacts extremes have are numerous. Economic impacts include closure of roads, outages of power grids, water shut-offs, and physical damage to buildings, bridges, crops and livestock (Jahn, 2015). Environmental impacts include coastal erosion, changes in water supply and land coverage (Seneviratne et al., 2012; Seddon et al., 2016; Seneviratne et al., 2021). Societal impacts include food and water availability, loss of life, increasing insurance costs and changes in property values (Morss et al., 2011; Bell et al., 2018; Zscheischler et al., 2018; Konapala et al., 2020). Extreme weather has intensified in recent decades, and will continue to have a disproportionately large impact on the environment, society and the economy (Seneviratne et al., 2021).

On a global scale, precipitation extremes are predicted to increase in intensity and frequency as the climate warms (e.g. Zhang et al., 2007; Min et al., 2011; Hirsch & Archfield, 2015). Work detailed in Kotz et al. (2022) has recently identified that increases in extreme rainfall reduce economic growth rates. A study by Pendergrass and Knutti (2018) investigated the uneven nature of precipitation, finding that half the annual precipitation occurs during the wettest 12 days of the year. When assessing output from CMIP5 climate models, they also found a shortening of the average number of days needed to reach half the annual precipitation highlighting the increased importance of extreme events.

65 Extra-tropical cyclones (hereafter referred to as cyclones) are key components of  
 66 the atmospheric general circulation due to their ability to transport large quantities of  
 67 heat, moisture, and momentum. Cyclones are an important contributor to extreme weather  
 68 events as their passage is associated with strong winds, precipitation, and temperature  
 69 changes (Papritz et al., 2014). Studies quantifying cyclone-associated precipitation find  
 70 that up to 90% of precipitation in the mid-latitude storm tracks is associated with frontal  
 71 systems and their associated cyclones (Catto et al., 2012; Hawcroft et al., 2012; Utsumi  
 72 et al., 2017). Pfahl and Wernli (2012) has also identified that a high percentage of pre-  
 73 cipitation extremes are directly related to cyclones, with some locations having up to 80%  
 74 of their precipitation extremes associated with cyclones. Utsumi et al. (2017) also iden-  
 75 tify that large amounts of extreme precipitation in mid-latitude regions are associated  
 76 with cyclones. McErlich, McDonald, Schuddeboom, et al. (2023) has also recently demon-  
 77 strated that larger precipitation extremes are associated with regions where large scale  
 78 precipitation processes, such as cyclones, dominate.

79 In this study we use a regionally dependent precipitation threshold to classify pre-  
 80 cipitation extremes relative to the cyclone centre. Cyclone composites for both average  
 81 and extreme precipitation are calculated from the ERA5 reanalysis. Composites are then  
 82 partitioned into different stages of the lifecycle to assess the spatial and temporal evo-  
 83 lution of extremes. The rate at which extremes precipitation changes throughout the cy-  
 84 clone lifecycle is then quantified.

## 85 2 Datasets and Methods

### 86 2.1 ERA5

87 We use output from the ERA5 reanalysis to identify cyclones over the Southern  
 88 Hemisphere for the years 1980 - 2019 inclusive. ERA5 is available on a  $0.25^\circ$  latitude/longitude  
 89 grid and at an hourly temporal resolution, however three hourly data was used in this  
 90 study. Previous work (McDonald & Cairns, 2020; McErlich, McDonald, Schuddeboom,  
 91 et al., 2023; McErlich, McDonald, Renwick, & Schuddeboom, 2023) shows that ERA5  
 92 is consistent with a number of satellite and reanalysis datasets for determining precip-  
 93 itation. This past research also shows that ERA5 can be used to successfully examine  
 94 cyclonic structure within a compositing framework for 10m wind speeds, total column  
 95 water vapour, cloud liquid water, and precipitation.

### 96 2.2 Cyclone tracking and compositing methodology

97 Work by Crawford and Serreze (2016) introduces and details the mean sea level  
 98 pressure (MSLP) based cyclone tracking algorithm used in this study. Previous work in  
 99 McErlich, McDonald, Renwick, and Schuddeboom (2023) also describes application of  
 100 the cyclone tracking algorithm over the Southern Hemisphere using ERA5, but a short  
 101 summary is included in the following paragraphs.

102 Local minima in the ERA5 mean sea level pressure (MSLP) field are used to iden-  
 103 tify cyclone centres. This covers the time period between 1980 - 2019 with a temporal  
 104 resolution of three hour and cyclones are identified using local minima in the MSLP field.  
 105 A radius-based threshold is also used to identify whether it is a closed low pressure sys-  
 106 tem, and thus can be characterised as a cyclone. A maximum propagation speed of  $150$   
 107  $\text{kmhr}^{-1}$  is used to join related low pressure centres into continuous cyclone tracks. Cri-  
 108 teria are also applied to reject systems that have a lifespan shorter than 24 hours, a track  
 109 length less than 100km, or do not spend some part of their lifetime at latitudes south  
 110 of  $30^\circ\text{S}$ . This causes cyclone tracks to predominately be concentrated over the South-  
 111 ern Ocean (not shown; see Figure 1 McErlich, McDonald, Renwick, & Schuddeboom, 2023);  
 112 This is in agreement with previous research that analyzed Southern hemisphere cyclone  
 113 tracks (e.g. Hoskins & Hodges, 2005; Bengtsson et al., 2006; Hodges et al., 2011).

The identified cyclone centers are then used to transform ERA5 data into a cyclone centered-coordinate system in the form of cyclone composites as detailed in McErlich, McDonald, Renwick, and Schuddeboom (2023). Cyclone composites are calculated using a radius of 2000 km, which is commonly used in previous work (e.g. Field & Wood, 2007; Field et al., 2008; Naud et al., 2012; Booth et al., 2018; McErlich, McDonald, Renwick, & Schuddeboom, 2023). Individual composites are rotated so that the direction of propagation of the cyclone is chosen to be travelling eastward. Given the zonal westerly winds over the Southern Ocean many cyclones require little rotation. This step approximately aligns the position of the warm/cold fronts and the area of warm, moist air associated with them. While not all fronts will be at the same position relative to the direction of the cyclone, this rotation acts to focus the structure of the composite (Govekar et al., 2011).

### 2.3 Analysis of cyclone lifecycle

To better understand changes in precipitation as the cyclone evolves, we partition the cyclones into three distinct developmental phases. We classify cyclones relative to the time of their maximum depth, which is defined as the time of maximum difference between the edge pressure and central pressure of the cyclone. We define three phases to represent periods of deepening, peak intensity and decay within the cyclone. The phase of peak intensity is defined as 6 hours either side of the time of maximum depth. The deepening phase is defined as measurements between 6 hours and 18 hours previous to the time of maximum depth. The decay phase is defined as measurements between 6 and 18 hours after the time of maximum depth.

In order to partition the cyclones into phases of deepening, peak intensity, and decay, a further criterion based on the deepening rate ( $\frac{\partial p}{\partial t}$ , scaled by latitude) was also assessed. Cyclone tracks were kept if the deepening rate changed from positive (indicating strengthening) during the deepening phase to negative (indicating weakening) during the decay phase. Cyclone track that pass this criterion are masked to only include data within the previously defined cyclone phases. Tracks without measurements 18 hours before and after the point of peak intensity are rejected, causing a minimum cyclone lifespan of 36 hours within the subset of cyclone tracks used in this analysis.

### 2.4 Identification of cyclone extremes associated with cyclones

In order to identify regions of the cyclone that correspond to precipitation extremes, we use a methodology introduced in McErlich, McDonald, Schuddeboom, et al. (2023). This produces regionally dependent thresholds for extreme precipitation which are then applied to a cyclone compositing framework. Firstly, a spatial map of precipitation wet day frequency is produced using a 1 mm/day threshold to define a wet day over the Southern hemisphere. This threshold is commonly used within the community (Polade et al., 2014; Schär et al., 2016) and is also used in a number of extreme precipitation indices as defined by the Expert Team on Climate Change Detection and Indices (ETCCDI; Zhang et al., 2011).

Secondly, rainfall data from regions of the same precipitation frequency are grouped together; This data is then aggregated to produce cumulative precipitation intensity distributions. McErlich, McDonald, Schuddeboom, et al. (2023) establishes this methodology forms coherent precipitation groupings, even through it connects spatially disparate regions together. The variability within wet day frequency regions has also been shown to be comparable to that within geographic regions.

Precipitation around the cyclone composite is then assessed to determine if it is an extreme for a given latitude/longitude based on the corresponding wet day frequency. Wet day frequency regions are identified within the cyclone composites using the geo-

163 graphic position of the cyclone centres, as determined by the tracking algorithm. A spa-  
 164 tially dependent threshold for precipitation extremes defined by the locations wet day  
 165 frequency is then applied to the cyclone composites, removing data below the  $n$ th per-  
 166 centile value of the aggregated precipitation. This process is repeated across each wet  
 167 day frequency region to account for changes in the underlying processes that generate  
 168 precipitation. This methodology produces masked cyclone composites consisting of only  
 169 precipitation at locations where it is above the spatially dependent  $n$ th percentile thresh-  
 170 old.

171 Setting this threshold to the upper tail of the precipitation distribution determines  
 172 cyclone composites for the extremes. Here we assess both the 90th and the 98th percentiles  
 173 allowing us to examine precipitation extremes. We also mask precipitation by a 1 mm  
 174 per day wet day threshold (Zhang et al., 2011) and 50th percentile value. While not in-  
 175 dicative of extremes, these sets of composites provide data which the extreme compos-  
 176 ites can be compared with, allowing us to understand unique features associated with  
 177 extreme precipitation. We note that the wet day frequency has a narrower range (see  
 178 Figure 1 McErlich, McDonald, Schuddeboom, et al., 2023) over the Southern Ocean where  
 179 the concentration of cyclones is the highest. This means there will be less variability in  
 180 the extreme precipitation thresholds over the Southern Ocean than for a global analy-  
 181 sis.

### 182 **3 Results**

183 Figure 1 shows the occurrence of precipitation for the wet day precipitation, 50th,  
 184 90th and 98th percentile masked composites in the cyclone centered coordinate system.  
 185 Here precipitation occurrence is defined within each masked subset of composites as the  
 186 percentage of time precipitation is identified. To highlight the changes in the structure,  
 187 each set of composites are shown on different colour scales. Because of the rotation ap-  
 188 plied to the cyclone composites, the top of the composites may not align with north, so  
 189 cardinal directions are not used to describe cyclone features.

190 Figure 1a-c shows the precipitation occurrence for the wet day precipitation dur-  
 191 ing the deepening phase, with rates up to 100% relative to the cyclone. Occurrence then  
 192 decreases slightly throughout the cyclone lifecycle. Given the potential for significant di-  
 193 abatic heating/latent heat release during the deepening phase (Wernli et al., 2002; Lud-  
 194 wig et al., 2014; Binder et al., 2016; Messmer & Simmonds, 2021) this pattern is expected.  
 195 The spatial structure shows high precipitation occurrence about the cyclone centre, that  
 196 extends in a tail towards the left side of the composite. This tail rotates clockwise through-  
 197 out the lifecycle, likely highlighting the warm seclusion identified in idealised models.

198 Looking at the 50th percentile masked composites, Figure 1d-f similarly shows high-  
 199 est precipitation occurrence during the deepening phase, of up to 80%, before decreas-  
 200 ing in later lifecycle stages. The spatial region associated with high occurrences shows  
 201 a reduced extent from that seen in 1a-c, with a more pronounced comma structure in  
 202 the upper left quadrant of the cyclone. This comma structure in precipitation has long  
 203 been identified in conceptual models of cyclones (see Semple, 2003) and is likely related  
 204 to the warm conveyor belt. This comma rotates clockwise as the cyclone evolves and the  
 205 drier poleward area of the cyclone moves equatorward towards the cyclone centre.

206 Comparable patterns are observed when looking at the 90th percentile masked cy-  
 207 clone composites for extreme precipitation occurrence (Figure 1g-i) and the 98th per-  
 208 centile masked composites (Figure 1j-l). Precipitation occurrence is once again great-  
 209 est during deepening, before decreasing in the peak intensity and decay phases. The struc-  
 210 ture of the high occurrence comma also rotates clockwise through the cyclone lifecycle.  
 211 A further reduction in the spatial extent of high occurrence regions from Figure 1d-f is  
 212 observed, such that the occurrence of precipitating extremes outside the comma is very

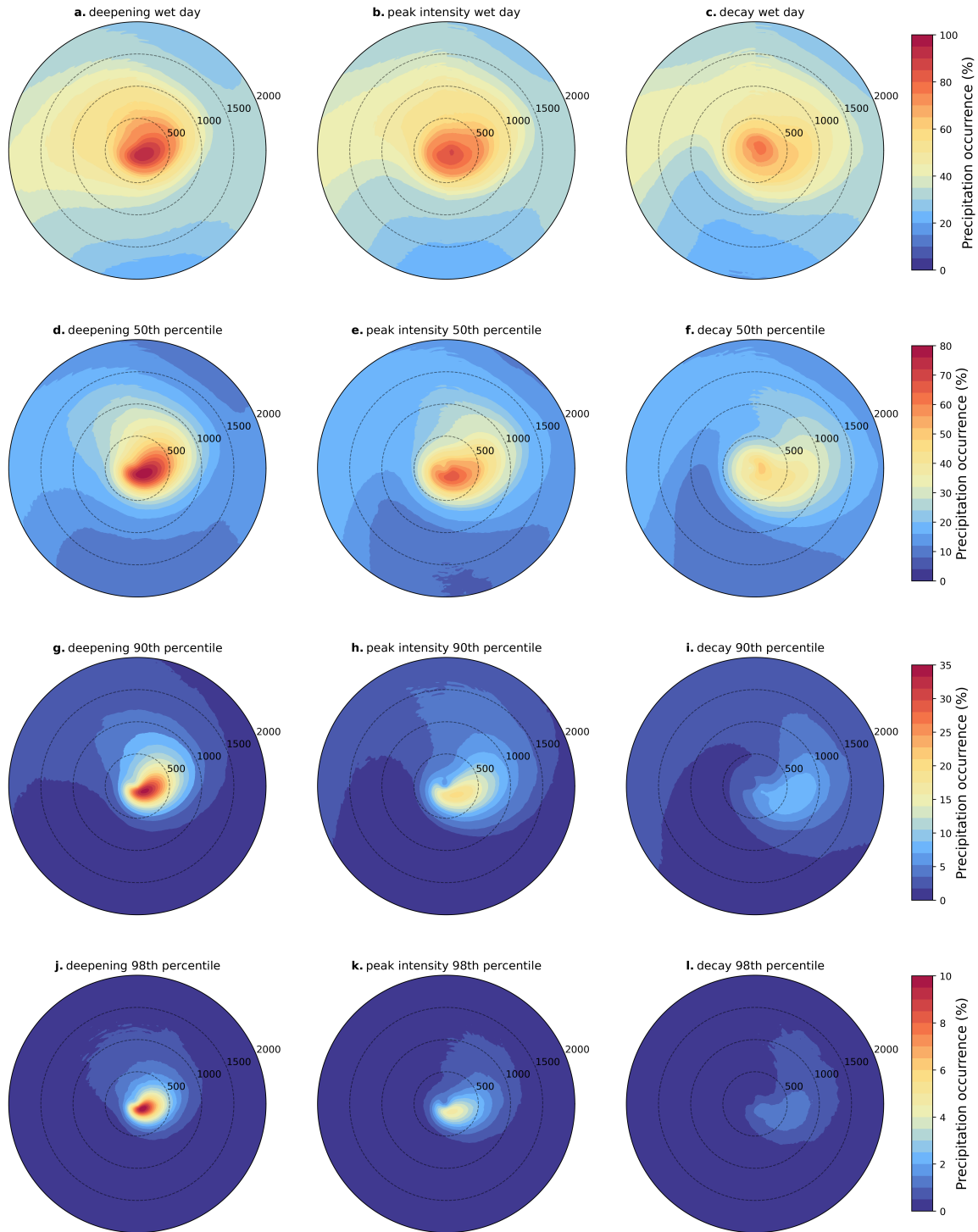


**Figure 1.** ERA5 cyclone composites of precipitation occurrence between 1980 - 2019 broken into the deepening, peak intensity and decay phases for (a - c) wet day precipitation (d - f) precipitation masked by the 50th percentile value (g - i) precipitation masked by the 90th percentile value (k - l) precipitation masked by the 98th percentile value.

213 low. For the 90th percentile masked composites precipitation extremes rarely occur within  
 214 the drier poleward region of the cyclone; For the 98th percentile masked composites pre-  
 215 cipitation extremes rarely occur outside of the comma structure.

216 To examine extreme precipitation from a different perspective, the fraction of the  
 217 total precipitation fraction associated with each threshold is derived in Figure 2. This  
 218 fraction is defined as the ratio of precipitation accumulated above a given threshold and  
 219 the total accumulated precipitation (Supplementary Figure 1). For the wet day percentiles,  
 220 this accumulation is determined using a 1 mm per day threshold. The  $n$ th percentile thresh-  
 221 old is used for the 50th, 90th and 98th percentile masked cyclone composites. Figure 2  
 222 shows precipitation fraction calculated for each point across the cyclone composite, for  
 223 the wet day precipitation and 50th, 90th and 98th percentile masked composites. Note  
 224 the different colour scales on each row of subplots used to distinguish structure.

225 Figure 2a-c shows areas within the cyclone composites where almost 100% of pre-  
 226 cipitation is above the 1 mm wet day threshold. Higher precipitation fraction is concen-  
 227 trated in the comma region of the cyclone composite and in the warm equatorward re-  
 228 gion of the cyclone. Precipitation fraction is greatest during the deepening phase, de-  
 229 creases and rotates clockwise in the peak intensity phase, then weakens during the de-  
 230 cay phase. The area of lowest precipitation fraction occurs in the cold poleward region  
 231 of the composite, where more of the rainfall is below the 1 mm wet day threshold sug-  
 232 gesting a region dominated by drizzle. This region moves equatorward up the left flank  
 233 of the cyclone into the upper left quadrant as the cyclone evolves. An almost identical  
 234 pattern is seen for the 50th percentiles masked composites on Figure 2d-f. Differences  
 235 include a lesser precipitation fraction, and a reduced spatial extent similar to that seen  
 236 between Figure 1a-c and d-f.

237 When looking at the precipitation fraction for the 90th percentile masked compos-  
 238 ites, Figure 2g-i shows a decrease compared to the 50th percentile threshold as would  
 239 be expected. The fraction of the total precipitation linked to events above this thresh-  
 240 old are still highest during the deepening phase, but the greatest precipitation fraction  
 241 (almost 80%) is lower compared to Figure 2a/d. That up to 80% of precipitation is as-  
 242 sociated with the top 10% of the precipitation distribution is meaningful, and highlights  
 243 the importance of cyclones for extreme precipitation in general. Regions of high precip-  
 244 itation fraction are more concentrated in the centre of the cyclone compared to Figure  
 245 2a-f, but with a broad region of 40% to 50% precipitation fraction within the equator-  
 246 ward region of the cyclone highlighting the importance of extreme precipitation in the  
 247 overall accumulation. A clockwise rotation in regions of highest precipitation fraction  
 248 is also observed throughout the cyclone evolution, as the precipitation fraction weakens  
 249 throughout the peak intensity and decay phases.

250 When applying the strictest threshold and masking by the 98th percentile value,  
 251 Figure 2j-l shows a further decrease in the fraction of the total precipitation associated  
 252 with events above this threshold. Though, the greatest precipitation fraction is close to  
 253 50% and occurs during the deepening phase, before a reduction and clockwise rotation  
 254 is seen similar to Figure 2g-i. Structurally the large precipitation fraction shows the small-  
 255 est extent at the 98th percentile, being most concentrated within the comma region of  
 256 near the cyclone centre.

257 Results observed for the precipitation occurrence and fraction show similarities in  
 258 structure between the masked cyclone composites. Figure 3a-b shows the Pearson cor-  
 259 relation coefficients and spatial averages for the precipitation fraction across the cyclone  
 260 composite as shown on Figures 1 and 2. Correlation is calculated pairwise between each  
 261 set of cyclone composites, spatially across the composite. Results also show that precip-  
 262 itation is greatest during the deepening phase, and then weakens as the cyclone evolves.  
 263 However, Figures 1 - 2 show this weakening happens at different rates. To investigate  
 264 the similarities between the cyclone composites and to quantify this weakening, the ra-

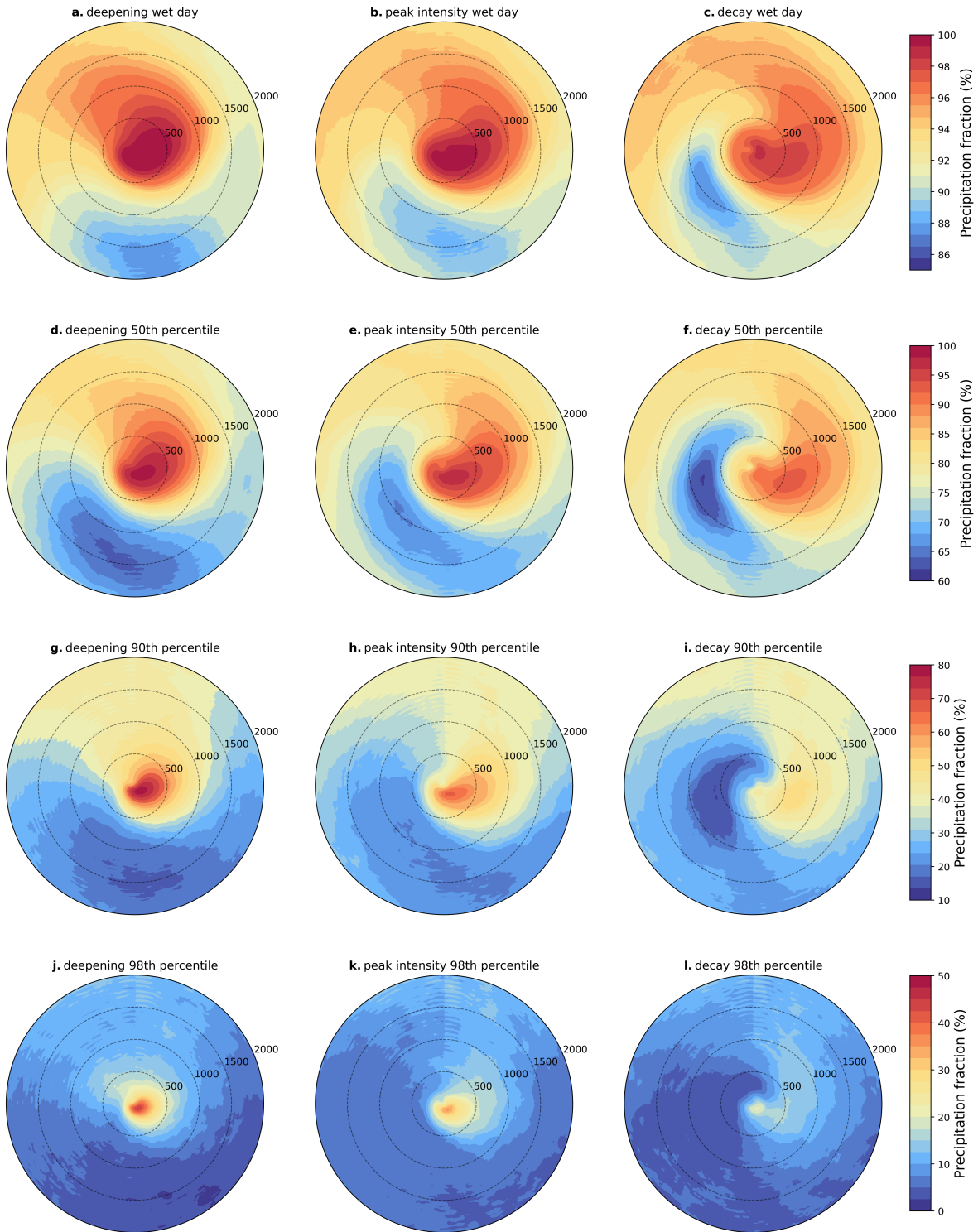


**Figure 2.** ERA5 cyclone composites of precipitation fraction between 1980 - 2019 broken into the deepening, peak intensity and decay phases for (a - c) wet day precipitation (d - f) precipitation masked by the 50th percentile value (g - i) precipitation masked by the 90th percentile value (k - l) precipitation masked by the 98th percentile value.

265 tio of the averages in the peak intensity and decay phases relative to the deepening phase  
 266 are also shown in Figure 3c-d.

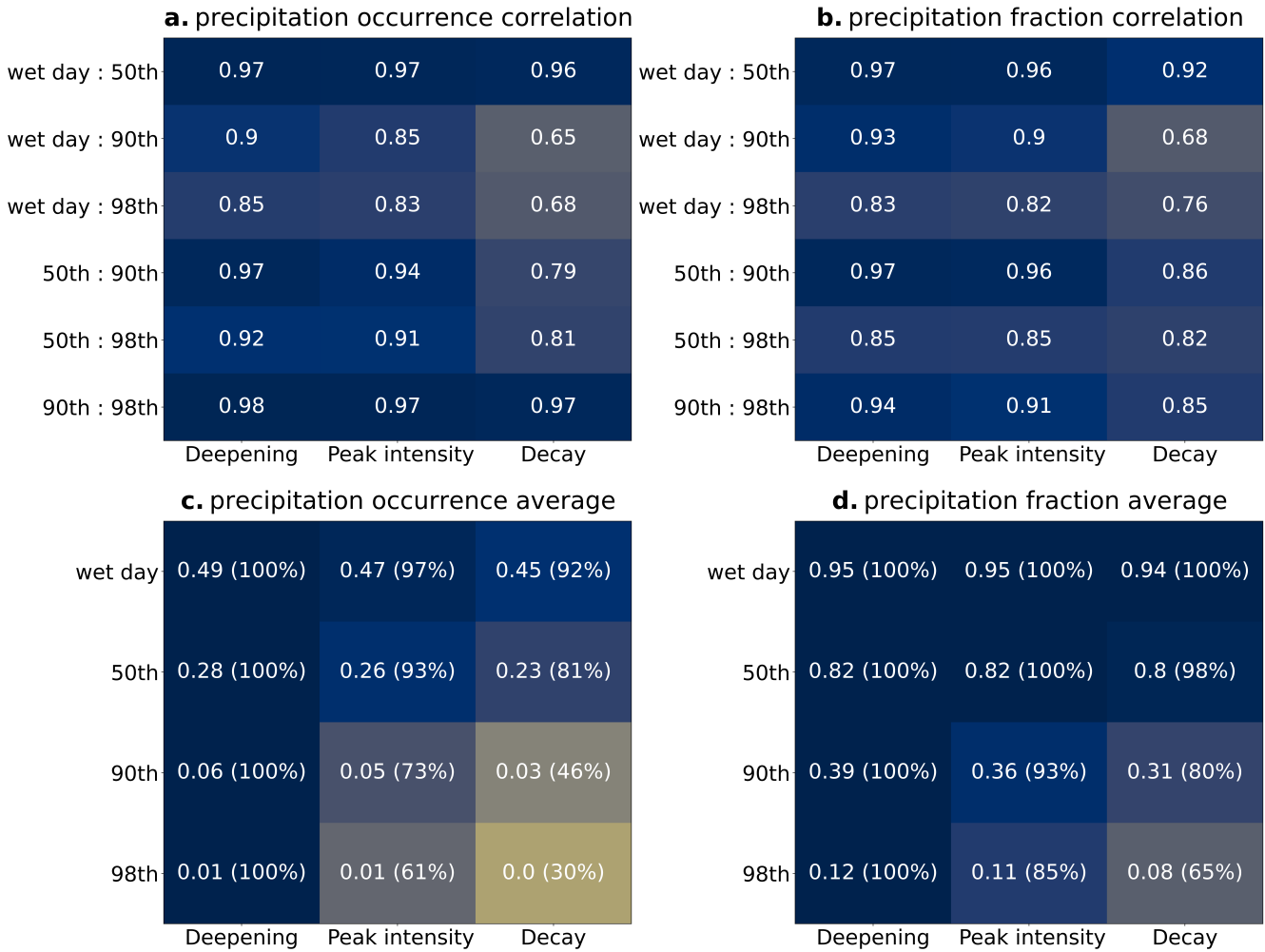


**Figure 3.** a) Pairwise Pearson correlation coefficients for cyclone composites within the deepening, peak intensity and decay phases for the precipitation occurrence b) same as a) but for precipitation fraction c) Precipitation averages across the cyclone composites within the deepening, peak intensity and decay phases for the precipitation occurrence d) same as c) but for precipitation fraction. The bracketed percentages for (c - d) indicate precipitation averages as a proportion of the corresponding deepening phase value.

267 Pairwise spatial correlations for the precipitation occurrence (Figure 3a) show strong  
 268 agreement between each masked composites at the same period in the cyclone lifecycle.  
 269 Correlation is strongest during the deepening phase in all cases. Correlation is lowest  
 270 between the wet day precipitation and 90/98th percentile masked composites, but still  
 271 strong within the deepening phase. When comparing the wet day precipitation/50th per-  
 272 centiles and 90th/98th masked composites, the spatial correlation remains consistently  
 273 high across the cyclone lifecycle. When looking at the precipitation fraction, the pair-  
 274 wise correlation shows a similar trend to that observed for the precipitation occurrence.  
 275 There is a strong correlation during the deepening phase and weaker correlation during  
 276 the decay phase.

277 Looking at the average precipitation occurrence across the cyclone (Figure 3c), not  
 278 only do the extremes have lower occurrence than the non-extreme precipitation, but drop  
 279 off significantly faster. The wet day precipitation and 50th percentile masked compos-  
 280 ites decrease to 90% and 81% of the deepening value during the decay phase, respectively.  
 281 The 90th percentile composites decrease to 46% of the deepening value and the 98th per-  
 282 centile composites to 30% of the deepening value during the decay phase. This indicates  
 283 as you increase the threshold for determining extremes, they will be disproportionately  
 284 be experienced most often during the deepening phase, as the occurrence weakens greatly  
 285 by the decay phase. Averages for the precipitation fraction (Figure 3d) display a sim-  
 286 ilar trend. The 90th and 98th percentile masked composites decrease to 80% and 65%  
 287 of the deepening value, respectively, while the wet day precipitation and 50th percentile  
 288 masked composites decrease negligibly. This highlights that as you increase the thresh-  
 289 old for the extremes the deepening phase becomes more important, as a lower propor-  
 290 tion of the total precipitation experienced in future cyclone phases can be defined as ex-  
 291 treme.

## 292 4 Discussion and Conclusion

293 Using a spatially dependent threshold for precipitation, we have developed a sim-  
 294 ple methodology to assess the contribution to accumulation and the occurrence of pre-  
 295 cipitation extremes by masking data within a cyclone compositing framework. This method-  
 296 ology is based on grouping regions of similar precipitation frequency together, which have  
 297 been shown to be influenced by the same underlying dynamic and thermodynamic pre-  
 298 cipitation processes (McErlich, McDonald, Schuddeboom, et al., 2023). While some past  
 299 studies investigate precipitation extremes and how they connect to cyclones (e.g. Pfahl  
 300 & Wernli, 2012; Catto & Dowdy, 2021; Messmer & Simmonds, 2021), this is the first in-  
 301 vestigation from a cyclone centered perspective over the Southern Hemisphere, instead  
 302 of focusing on assessing the spatial distributions of cyclones.

303 Here we see that the greatest precipitation occurrence and fraction of total precip-  
 304 itation occur before the cyclone reaches its peak intensity. The precipitation accumu-  
 305 lation (Supplementary Figure 1) is also greatest during the deepening phase, meaning  
 306 precipitation extremes will be experienced most acutely during the deepening phase. This  
 307 is not a new result, as Booth et al. (2018) and McErlich, McDonald, Renwick, and Schud-  
 308 deboom (2023) also show that greater precipitation occurs before the cyclone reaches peak  
 309 intensity. These studies also show a weakening in the comma structure of precipitation  
 310 through the cyclone lifecycle. However, we show that extreme precipitation also displays  
 311 a similar trend. For both the 90th and 98th masked percentile composites, the precip-  
 312 itation occurrence and fraction is greatest during the deepening phase and then decays  
 313 slightly as the cyclone evolves. Many studies have shown support for the concept that  
 314 the release of latent heating associated with precipitation leads to the intensification of  
 315 a cyclone (Wernli et al., 2002; Ludwig et al., 2014; Binder et al., 2016; Messmer & Sim-  
 316 monds, 2021), which is consistent with our findings.

317 Figure 3c-d shows that precipitation occurrence and precipitation fraction weak-  
 318 ens at a faster rate as you increase from the 90th to 98th percentile of precipitation. This  
 319 suggests a larger diabatic heating and subsequent intensification of the cyclone from ex-  
 320 treme precipitation events. Figure 3c-d also shows that the precipitation occurrence shows  
 321 a larger change from the deepening to the decay phase than the precipitation fraction  
 322 at every extreme threshold. This suggests that during the decay phase a larger amount  
 323 of rainfall is associated with a smaller number of extreme events.

324 Looking at the spatial pattern of precipitation within cyclone composites, Figures  
 325 1 and 2 show that as you apply a stricter threshold to mask precipitation there is a re-  
 326 duction in the spatial extent of both high precipitation occurrence and fraction. As you

327 move towards the extremes, precipitation is more concentrated towards the centre of the  
328 cyclone within the comma region linked to the warm conveyor belt.

329 Figure 3a-b shows that for the precipitation occurrence and fraction, the 90th and  
330 98th percentile masked composites show strong spatial correlation across all states of the  
331 cyclone lifecycle. The wet day precipitation and 50th and 90th/98th percentile masked  
332 cyclone composites shows strong agreement for precipitation occurrence and fraction dur-  
333 ing the deepening and peak intensity phases, but weaker agreement during the decay phase.  
334 These correlations show that the spatial regions of the cyclone where precipitation ex-  
335 tremes are important remain similar across the cyclone lifecycle, suggesting that know-  
336 ing the median precipitation pattern could provide insight into the upper tail of the dis-  
337 tributions, at least for the precipitation occurrence and fraction.

338 This work has determined the spatial structure of extreme precipitation relative  
339 to cyclone centres, and provided a quantification of how these extremes change as the  
340 cyclone evolves. However, the underlying processes that determine precipitation have not  
341 been assessed to provide a physical justification for results seen in this work. McErlich,  
342 McDonald, Schuddeboom, et al. (2023) has shown that vertical velocity and convective  
343 available potential energy are important drivers of global precipitation and that precip-  
344 itation is determined, in part, by the occurrence of these precipitation-generating pro-  
345 cesses. Future work will examine these processes to determine how they influence the  
346 behaviour of precipitation and precipitation extremes in cyclones through their life-  
347 cycle.

## 348 Acknowledgments

349 The ERA5 reanalysis products were obtained from the Copernicus Climate Data Store  
350 (<https://cds.climate.copernicus.eu/>). Data used to visualise the figures is available at  
351 <https://zenodo.org/record/7787119>. We would also like to acknowledge funding from the  
352 Ministry of Business, Innovation and Employment (MBIE), New Zealand, through the  
353 Whakahura project (grant number E7141).

## 354 References

- 355 Bell, J. E., Brown, C. L., Conlon, K., Herring, S., Kunkel, K. E., Lawrimore, J., ...  
356 Uejio, C. (2018). Changes in extreme events and the potential impacts on  
357 human health. *Journal of the Air & Waste Management Association*, 68(4),  
358 265-287. doi: 10.1080/10962247.2017.1401017
- 359 Bengtsson, L., Hodges, K. I., & Roeckner, E. (2006). Storm tracks and climate  
360 change. *Journal of Climate*, 19(15), 3518 - 3543. Retrieved from [https://](https://journals.ametsoc.org/view/journals/clim/19/15/jcli3815.1.xml)  
361 [journals.ametsoc.org/view/journals/clim/19/15/jcli3815.1.xml](https://journals.ametsoc.org/view/journals/clim/19/15/jcli3815.1.xml) doi:  
362 10.1175/JCLI3815.1
- 363 Binder, H., Boettcher, M., Joos, H., & Wernli, H. (2016). The role of warm con-  
364 veyor belts for the intensification of extratropical cyclones in northern hemi-  
365 sphere winter. *Journal of the Atmospheric Sciences*, 73(10), 3997 - 4020. doi:  
366 10.1175/JAS-D-15-0302.1
- 367 Booth, J. F., Naud, C. M., & Jeyaratnam, J. (2018). Extratropical cyclone pre-  
368 cipitation life cycles: A satellite-based analysis. *Geophysical Research Let-*  
369 *ters*, 45(16), 8647-8654. Retrieved from [https://agupubs.onlinelibrary](https://agupubs.onlinelibrary.wiley.com/doi/abs/10.1029/2018GL078977)  
370 [.wiley.com/doi/abs/10.1029/2018GL078977](https://agupubs.onlinelibrary.wiley.com/doi/abs/10.1029/2018GL078977) doi: [https://doi.org/10.1029/](https://doi.org/10.1029/2018GL078977)  
371 [2018GL078977](https://doi.org/10.1029/2018GL078977)
- 372 Catto, J. L., & Dowdy, A. (2021). Understanding compound hazards from a  
373 weather system perspective. *Weather and Climate Extremes*, 32, 100313.  
374 Retrieved from [https://www.sciencedirect.com/science/article/pii/](https://www.sciencedirect.com/science/article/pii/S2212094721000116)  
375 [S2212094721000116](https://www.sciencedirect.com/science/article/pii/S2212094721000116) doi: <https://doi.org/10.1016/j.wace.2021.100313>
- 376 Catto, J. L., Jakob, C., Berry, G., & Nicholls, N. (2012). Relating global precipita-

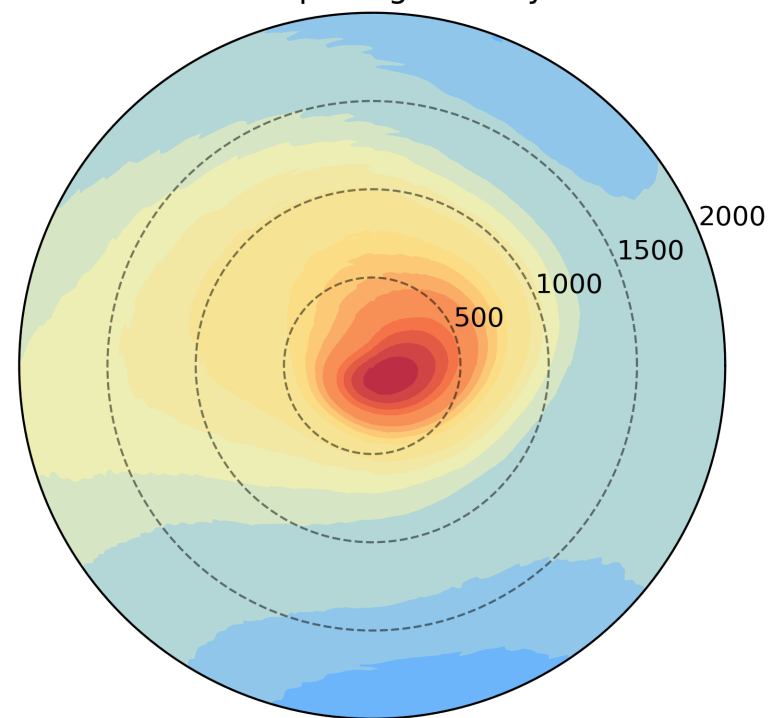
- tion to atmospheric fronts. *Geophysical Research Letters*, *39*(10). doi: <https://doi.org/10.1029/2012GL051736>
- Crawford, A. D., & Serreze, M. C. (2016). Does the summer arctic frontal zone influence arctic ocean cyclone activity? *Journal of Climate*, *29*(13), 4977 - 4993. doi: 10.1175/JCLI-D-15-0755.1
- Field, P. R., Gettelman, A., Neale, R. B., Wood, R., Rasch, P. J., & Morrison, H. (2008). Midlatitude cyclone compositing to constrain climate model behavior using satellite observations. *Journal of Climate*, *21*(22), 5887 - 5903. doi: 10.1175/2008JCLI2235.1
- Field, P. R., & Wood, R. (2007). Precipitation and cloud structure in midlatitude cyclones. *Journal of Climate*, *20*(2), 233 - 254. doi: 10.1175/JCLI3998.1
- Govekar, P. D., Jakob, C., Reeder, M. J., & Haynes, J. (2011). The three-dimensional distribution of clouds around southern hemisphere extratropical cyclones. *Geophysical Research Letters*, *38*(21). doi: <https://doi.org/10.1029/2011GL049091>
- Hawcroft, M., Shaffrey, L., Hodges, K., & Dacre, H. (2012, 12). How much northern hemisphere precipitation is associated with extratropical cyclones? *Geophysical Research Letters*, *39*, 24809-. doi: 10.1029/2012GL053866
- Hirsch, R. M., & Archfield, S. A. (2015, Mar 01). Not higher but more often. *Nature Climate Change*, *5*(3), 198-199. doi: 10.1038/nclimate2551
- Hodges, K. I., Lee, R. W., & Bengtsson, L. (2011). A comparison of extratropical cyclones in recent reanalyses era-interim, nasa merra, ncep cfsr, and jra-25. *Journal of Climate*, *24*(18), 4888 - 4906. Retrieved from <https://journals.ametsoc.org/view/journals/clim/24/18/2011jcli4097.1.xml> doi: 10.1175/2011JCLI4097.1
- Hoskins, B. J., & Hodges, K. I. (2005). A new perspective on southern hemisphere storm tracks. *Journal of Climate*, *18*(20), 4108 - 4129. doi: 10.1175/JCLI3570.1
- Howe, P. D., Boudet, H., Leiserowitz, A., & Maibach, E. W. (2014, Nov 01). Mapping the shadow of experience of extreme weather events. *Climatic Change*, *127*(2), 381-389. doi: 10.1007/s10584-014-1253-6
- Jahn, M. (2015). Economics of extreme weather events: Terminology and regional impact models. *Weather and Climate Extremes*, *10*, 29-39. doi: <https://doi.org/10.1016/j.wace.2015.08.005>
- Konapala, G., Mishra, A. K., Wada, Y., & Mann, M. E. (2020). Climate change will affect global water availability through compounding changes in seasonal precipitation and evaporation [Journal Article]. *Nature Communications*, *11*(1), 3044. doi: 10.1038/s41467-020-16757-w
- Kotz, M., Levermann, A., & Wenz, L. (2022, Jan 01). The effect of rainfall changes on economic production. *Nature*, *601*(7892), 223-227. doi: 10.1038/s41586-021-04283-8
- Ludwig, P., Pinto, J. G., Reyers, M., & Gray, S. L. (2014). The role of anomalous sst and surface fluxes over the southeastern north atlantic in the explosive development of windstorm xynthia. *Quarterly Journal of the Royal Meteorological Society*, *140*(682), 1729-1741. doi: <https://doi.org/10.1002/qj.2253>
- McDonald, A. J., & Cairns, L. H. (2020). A new method to evaluate reanalyses using synoptic patterns: An example application in the ross sea/ross ice shelf region. *Earth and Space Science*, *7*(1), e2019EA000794. Retrieved from <https://agupubs.onlinelibrary.wiley.com/doi/abs/10.1029/2019EA000794> doi: <https://doi.org/10.1029/2019EA000794>
- McErlich, C., McDonald, A., Renwick, J., & Schuddeboom, A. (2023). An assessment of southern hemisphere extra-tropical cyclones in era5 using windsat. *Au-thorea Preprints*. doi: 10.22541/essoar.167591115.54167961/v1
- McErlich, C., McDonald, A., Schuddeboom, A., Vishwanathan, G., Renwick, J., & Rana, S. (2023). Positive correlation between wet day frequency and intensity

- 432 linked to universal precipitation drivers. *Nature Geoscience*.
- 433 Messmer, M., & Simmonds, I. (2021). Global analysis of cyclone-induced com-  
 434 pound precipitation and wind extreme events. *Weather and Climate Extremes*,  
 435 32, 100324. doi: <https://doi.org/10.1016/j.wace.2021.100324>
- 436 Min, S.-K., Zhang, X., Zwiers, F. W., & Hegerl, G. C. (2011, Feb 01). Human con-  
 437 tribution to more-intense precipitation extremes. *Nature*, 470(7334), 378-381.  
 438 doi: 10.1038/nature09763
- 439 Morss, R. E., Wilhelmi, O. V., Meehl, G. A., & Dilling, L. (2011). Improving  
 440 societal outcomes of extreme weather in a changing climate: an integrated  
 441 perspective. *Annual Review of Environment and Resources*, 36, 1-25.
- 442 Naud, C. M., Posselt, D. J., & van den Heever, S. C. (2012). Observational analysis  
 443 of cloud and precipitation in midlatitude cyclones: Northern versus south-  
 444 ern hemisphere warm fronts. *Journal of Climate*, 25(14), 5135 - 5151. doi:  
 445 10.1175/JCLI-D-11-00569.1
- 446 Papritz, L., Pfahl, S., Rudeva, I., Simmonds, I., Sodemann, H., & Wernli, H.  
 447 (2014). The role of extratropical cyclones and fronts for southern ocean  
 448 freshwater fluxes. *Journal of Climate*, 27(16), 6205 - 6224. doi: 10.1175/  
 449 JCLI-D-13-00409.1
- 450 Pendergrass, A. G., & Knutti, R. (2018). The uneven nature of daily precipita-  
 451 tion and its change. *Geophysical Research Letters*, 45(21), 11,980-11,988.  
 452 Retrieved from [https://agupubs.onlinelibrary.wiley.com/doi/abs/](https://agupubs.onlinelibrary.wiley.com/doi/abs/10.1029/2018GL080298)  
 453 [10.1029/2018GL080298](https://doi.org/10.1029/2018GL080298) doi: <https://doi.org/10.1029/2018GL080298>
- 454 Pfahl, S., & Wernli, H. (2012). Quantifying the relevance of cyclones for precipita-  
 455 tion extremes. *Journal of Climate*, 25(19), 6770 - 6780. doi: 10.1175/JCLI-D  
 456 -11-00705.1
- 457 Polade, S. D., Pierce, D. W., Cayan, D. R., Gershunov, A., & Dettinger, M. D.  
 458 (2014, Mar 13). The key role of dry days in changing regional climate and  
 459 precipitation regimes. *Scientific Reports*, 4(1), 4364. doi: 10.1038/srep04364
- 460 Schär, C., Ban, N., Fischer, E. M., Rajczak, J., Schmidli, J., Frei, C., ... Zwiers,  
 461 F. W. (2016, Jul 01). Percentile indices for assessing changes in heavy  
 462 precipitation events. *Climatic Change*, 137(1), 201-216. doi: 10.1007/  
 463 s10584-016-1669-2
- 464 Seddon, A. W. R., Macias-Fauria, M., Long, P. R., Benz, D., & Willis, K. J. (2016,  
 465 Mar 01). Sensitivity of global terrestrial ecosystems to climate variability. *Na-  
 466 ture*, 531(7593), 229-232. doi: 10.1038/nature16986
- 467 Semple, A. (2003). A review and unification of conceptual models of cyclogenesis.  
 468 *Meteorological Applications*, 10, 39-59.
- 469 Seneviratne, S., Nicholls, N., Easterling, D., Goodess, C., S. Kanae, J. K., Luo, Y.,  
 470 ... Zhang, X. (2012). *Changes in climate extremes and their impacts on the  
 471 natural physical environment* (C. Field et al., Eds.). Cambridge, UK, and New  
 472 York, NY, USA: Cambridge University Press.
- 473 Seneviratne, S., Zhang, X., Adnan, M., Badi, W., Dereczynsk, C., Luca, A. D., ...  
 474 Zhou, B. (2021). *Weather and Climate Extreme Events in a Changing Climate*  
 475 (V. Masson-Delmotte et al., Eds.). Cambridge, UK, and New York, NY, USA:  
 476 Cambridge University Press.
- 477 Utsumi, N., Kim, H., Kanae, S., & Oki, T. (2017). Relative contributions of weather  
 478 systems to mean and extreme global precipitation. *Journal of Geophys-  
 479 ical Research: Atmospheres*, 122(1), 152-167. doi: [https://doi.org/10.1002/  
 480 2016JD025222](https://doi.org/10.1002/2016JD025222)
- 481 Wernli, H., Dirren, S., Liniger, M. A., & Zillig, M. (2002). Dynamical aspects  
 482 of the life cycle of the winter storm 'lothar' (24-26 december 1999). *Quar-  
 483 terly Journal of the Royal Meteorological Society*, 128(580), 405-429. doi:  
 484 <https://doi.org/10.1256/003590002321042036>
- 485 Zhang, X., Alexander, L., Hegerl, G. C., Jones, P., Tank, A. K., Peterson, T. C.,  
 486 ... Zwiers, F. W. (2011). Indices for monitoring changes in extremes based

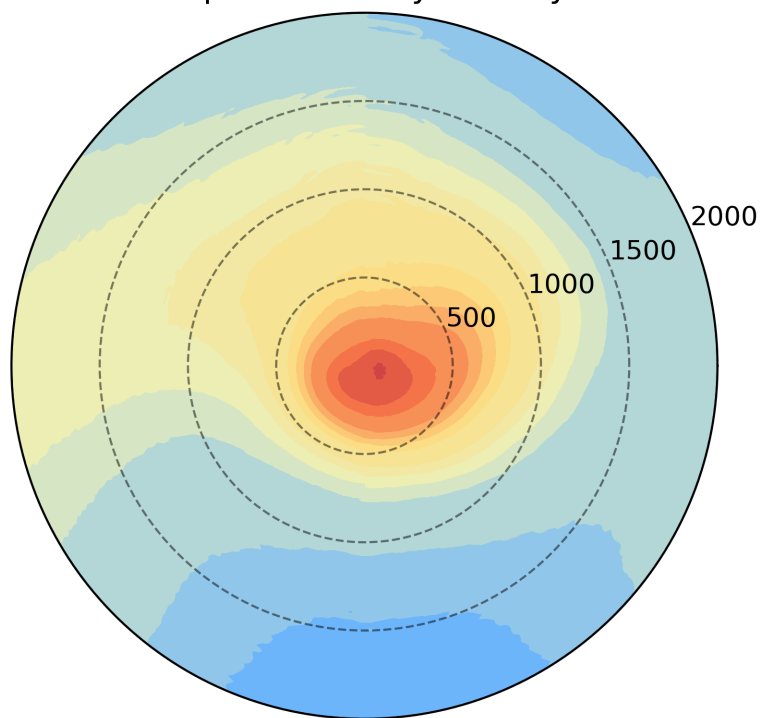
487 on daily temperature and precipitation data. *WIREs Climate Change*, 2(6),  
488 851-870. doi: 10.1002/wcc.147  
489 Zhang, X., Zwiers, F. W., Hegerl, G. C., Lambert, F. H., Gillett, N. P., Solomon,  
490 S., . . . Nozawa, T. (2007, Jul 01). Detection of human influence on  
491 twentieth-century precipitation trends. *Nature*, 448(7152), 461-465. doi:  
492 10.1038/nature06025  
493 Zscheischler, J., Westra, S., van den Hurk, B. J. J. M., Seneviratne, S. I., Ward,  
494 P. J., Pitman, A., . . . Zhang, X. (2018, Jun 01). Future climate risk  
495 from compound events. *Nature Climate Change*, 8(6), 469-477. doi:  
496 10.1038/s41558-018-0156-3

precipitation\_occurrence.png.

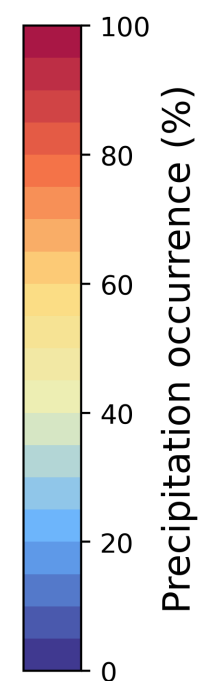
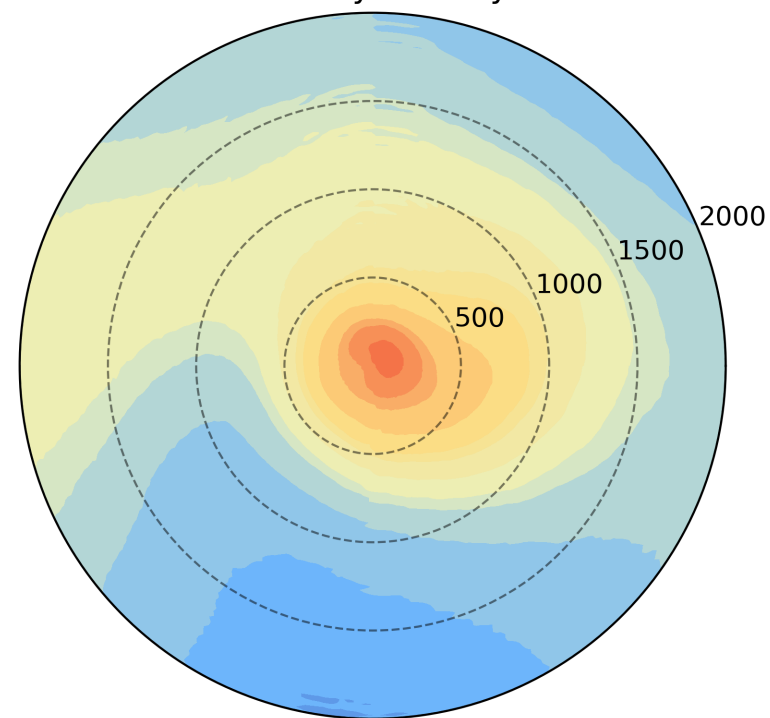
**a.** deepening wet day



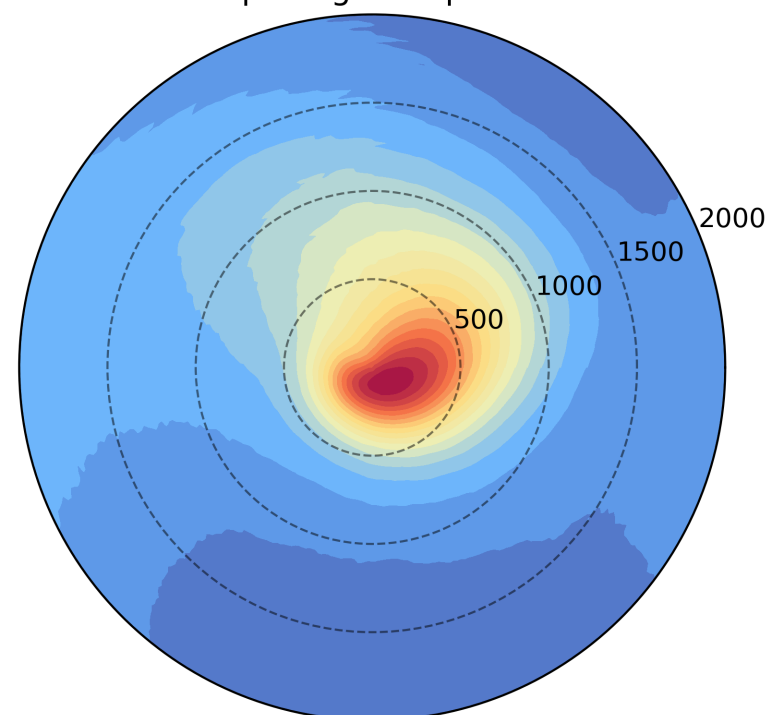
**b.** peak intensity wet day



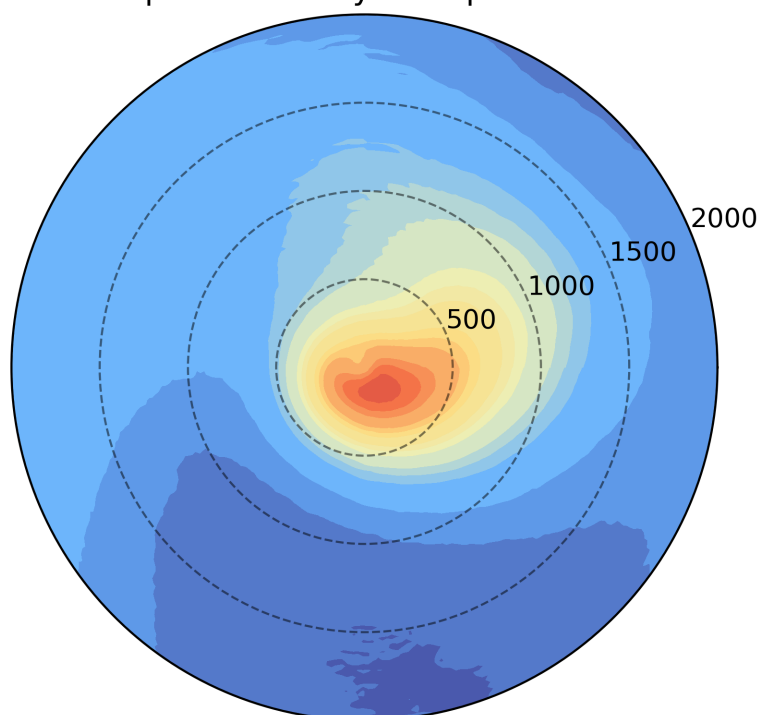
**c.** decay wet day



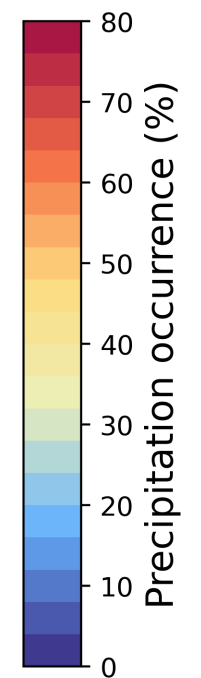
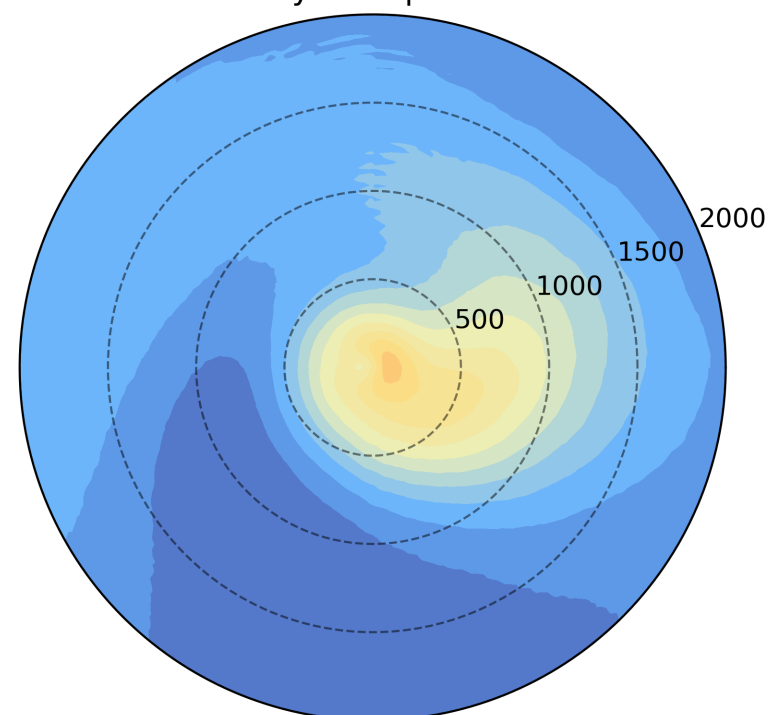
**d.** deepening 50th percentile



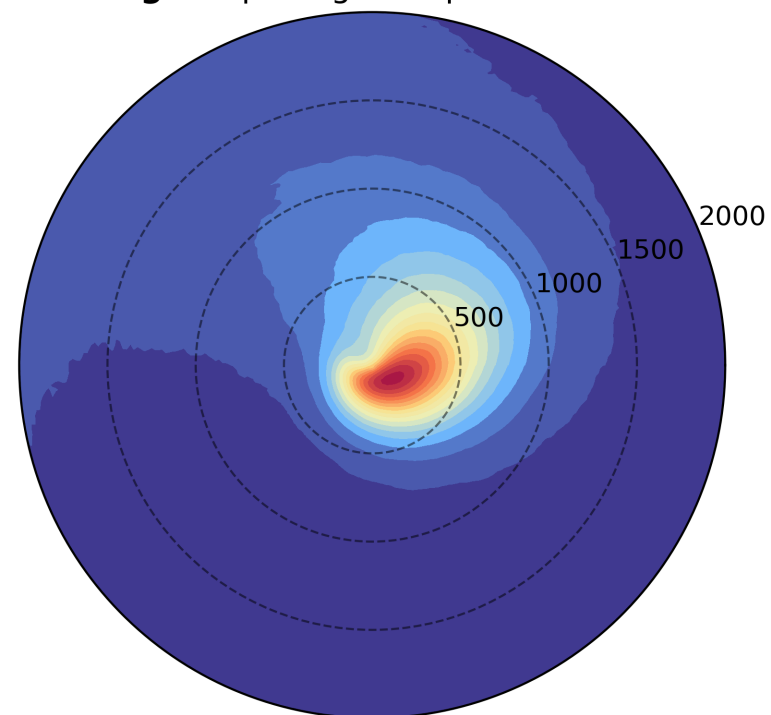
**e.** peak intensity 50th percentile



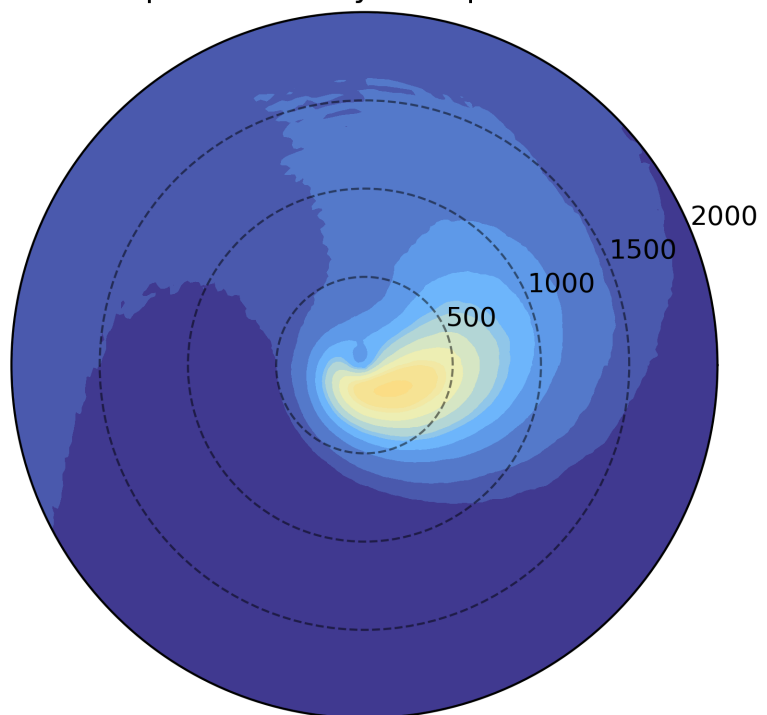
**f.** decay 50th percentile



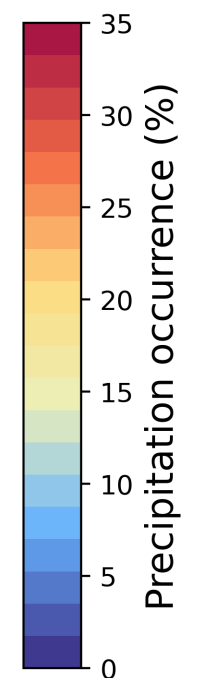
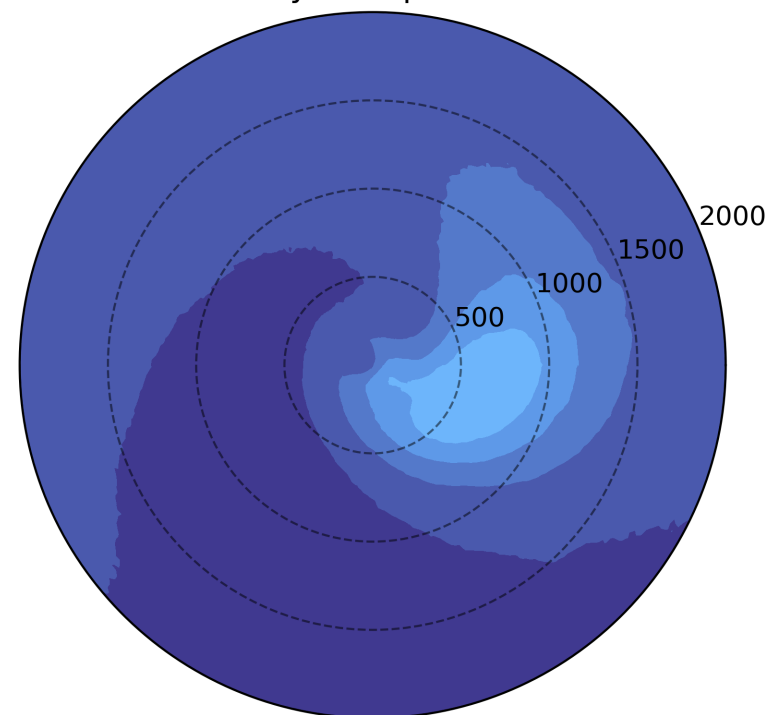
**g.** deepening 90th percentile



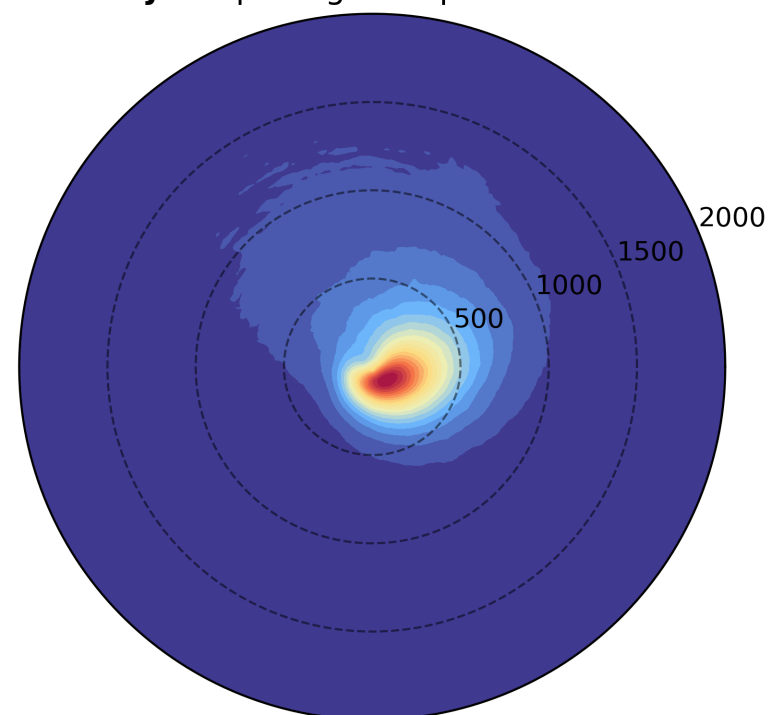
**h.** peak intensity 90th percentile



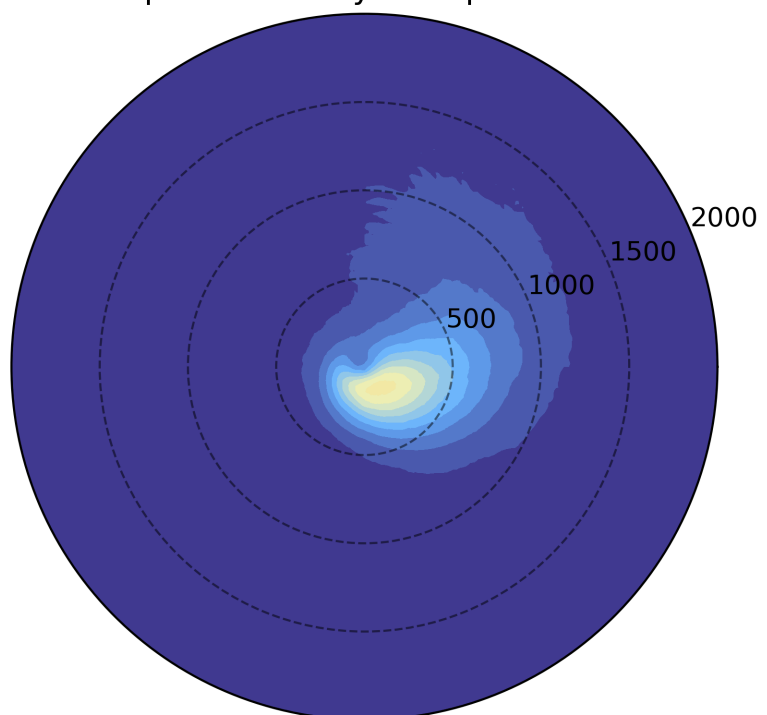
**i.** decay 90th percentile



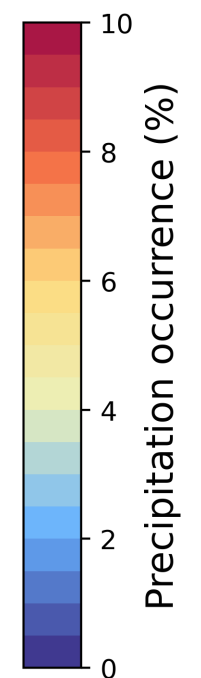
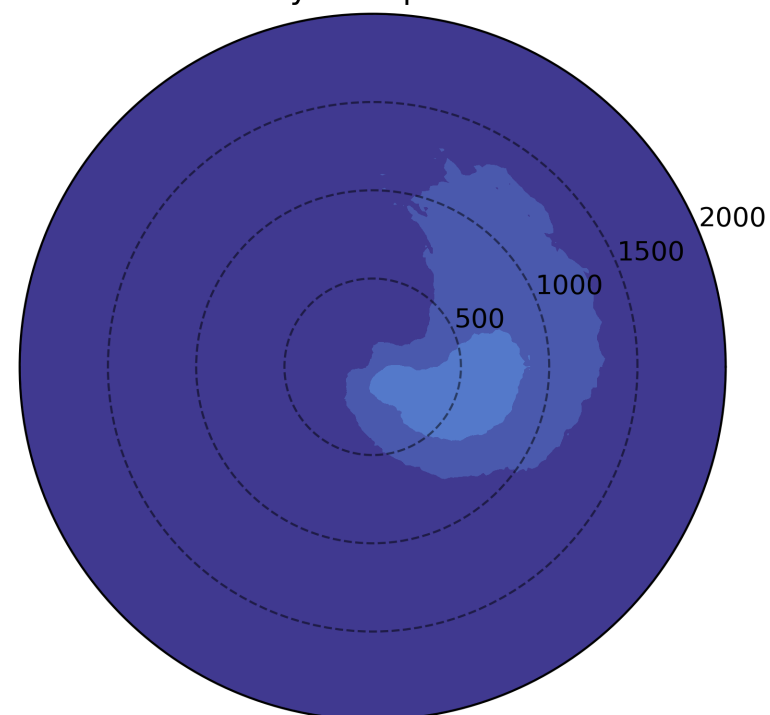
**j.** deepening 98th percentile



**k.** peak intensity 98th percentile

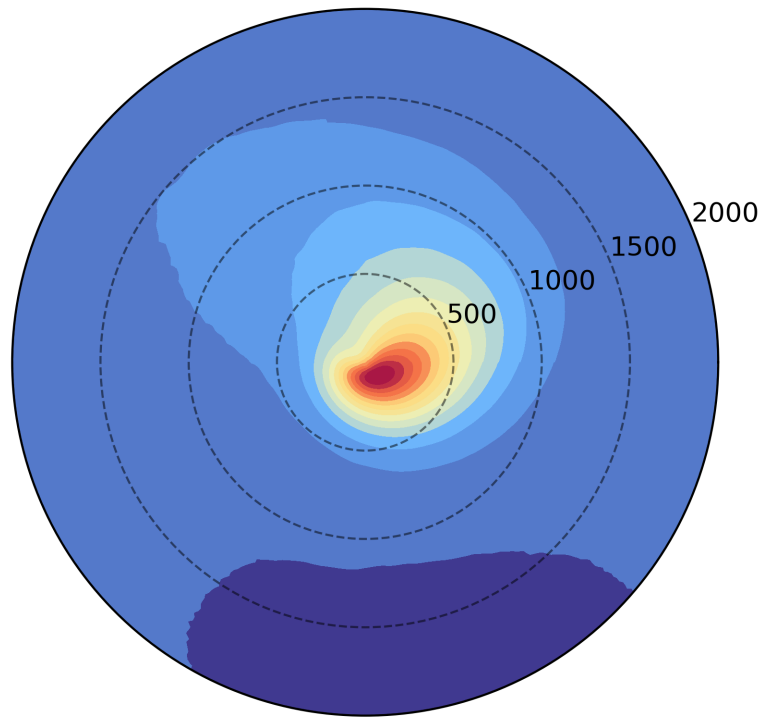


**l.** decay 98th percentile

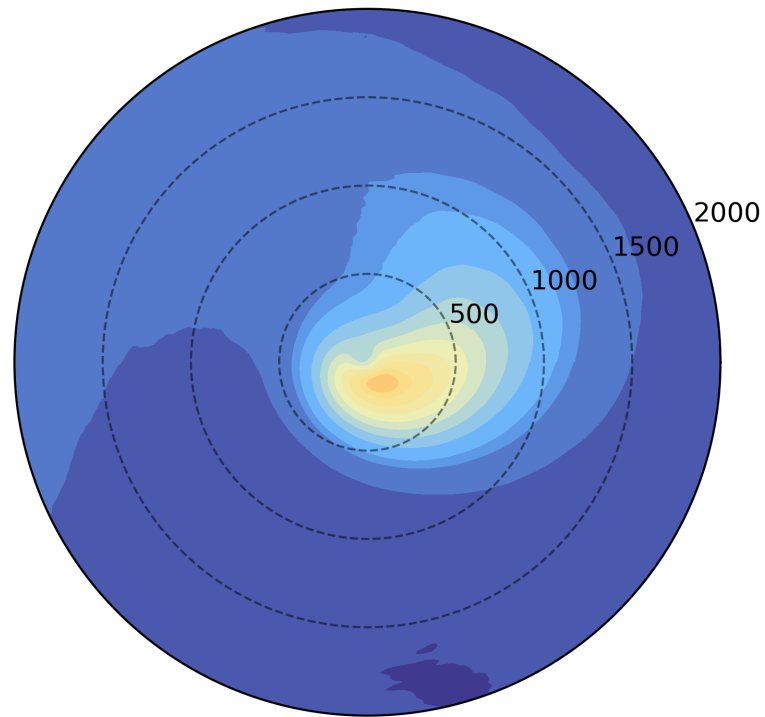


precipitation\_accumulation.png.

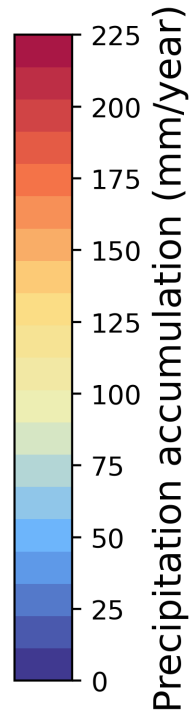
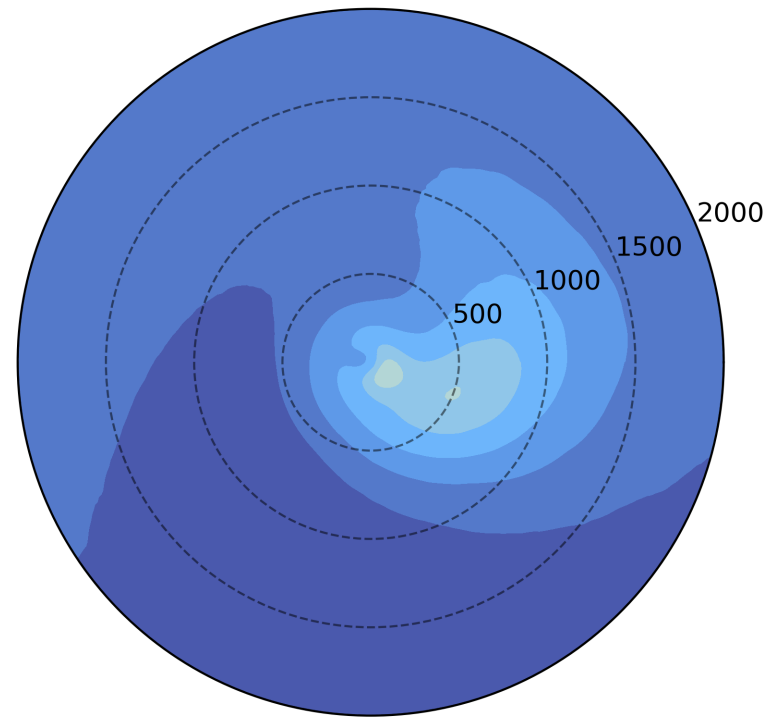
**a.** deepening accumulation



**b.** peak intensity accumulation



**c.** decay accumulation



precipitation\_fraction.png.



combined\_matrix.png.

**a. precipitation occurrence correlation**

wet day : 50th	0.97	0.97	0.96
wet day : 90th	0.9	0.85	0.65
wet day : 98th	0.85	0.83	0.68
50th : 90th	0.97	0.94	0.79
50th : 98th	0.92	0.91	0.81
90th : 98th	0.98	0.97	0.97
	Deepening	Peak intensity	Decay

**b. precipitation fraction correlation**

wet day : 50th	0.97	0.96	0.92
wet day : 90th	0.93	0.9	0.68
wet day : 98th	0.83	0.82	0.76
50th : 90th	0.97	0.96	0.86
50th : 98th	0.85	0.85	0.82
90th : 98th	0.94	0.91	0.85
	Deepening	Peak intensity	Decay

**c. precipitation occurrence average**

wet day	0.49 (100%)	0.47 (97%)	0.45 (92%)
50th	0.28 (100%)	0.26 (93%)	0.23 (81%)
90th	0.06 (100%)	0.05 (73%)	0.03 (46%)
98th	0.01 (100%)	0.01 (61%)	0.0 (30%)
	Deepening	Peak intensity	Decay

**d. precipitation fraction average**

wet day	0.95 (100%)	0.95 (100%)	0.94 (100%)
50th	0.82 (100%)	0.82 (100%)	0.8 (98%)
90th	0.39 (100%)	0.36 (93%)	0.31 (80%)
98th	0.12 (100%)	0.11 (85%)	0.08 (65%)
	Deepening	Peak intensity	Decay